11th World Congress on Computational Mechanics (WCCM XI)
5th European Conference on Computational Mechanics (ECCM V)
6th European Conference on Computational Fluid Dynamics (ECFD VI)
E. Oñate, J. Oliver and A. Huerta (Eds)

XFEM ANALYSIS OF TWO-DIMENSIONAL LAPLACE EQUATION WITH INCLINED SLIT BOUNDARIES

S. NAKASUMI[*] AND T. SUZUKI[†]

[*] Advanced Manufacturing Research Institute,
National Institute of Advanced Industrial Science and Technology (AIST),
East 1-2-1, Namiki, Tsukuba, Ibaraki, 305-8564, Japan,
e-mail: nakasumi.shogo@aist.go.jp
[†]Advanced Manufacturing Research Institute,
National Institute of Advanced Industrial Science and Technology (AIST),
East 1-2-1, Namiki, Tsukuba, Ibaraki, 305-8564, Japan,
email: suzuki-takayuki@aist.go.jp

Key Words: *XFEM, Laplace equation, Confomal mapping, Complex velocity potential.*

Abstract. In this research, a technique of XFEM which can analyze two-dimensional Laplace equation with slit type boundaries of arbitrary inclination angle is proposed. In this technique, a complex velocity potential in potential flow theory is used to represent the behaviour of potential around the slit. Namely, the real part of a complex power function is used as an enrich function. Distribution of potential obtained from a numerical example is verified by being decomposed into the classical finite element part and the enriched component part.

1 INTRODUCTION

XFEM is a numerical technique to model internal boundaries such as cracks, holes, interface of biomaterials, etc., without making the FEM mesh to conform to the geometries of structures[1-6]. The numerical framework is based on the concept of partition of unity[7]. The main characteristics added to the approximation of XFEM are discontinuity across the crack segment and singularity near the crack tip. The former is realized by the Heaviside step function and the latter is realized by the asymptotic crack-tip displacement field.

This technique has been mainly applied to the crack growth analysis of the structural member. For example, Sukumar et al. analyzed three dimensional fatigue crack propagation[8]. They also modeled holes and inclusions by level sets function[9]. Nagashima et al. applied the XFEM to the two-dimensional elastostatic bi-material interface cracks[10]. Elguedj proposed to use Hutchinson-Rice-Rosengren (HRR) fields to represent the singularities in elastic-plastic fracture mechanics[11]. As for fluid or fluid-structure interaction analysis, Sawada et al. applied XFEM to Navie-Stokes fluid analysis[12]. Gerstenberger and Wall presented XFEM using Lagrange multiplier based approach for fluid-structure interaction[13].

On the other hand, there are not so many studies of XFEM applied to the problems

described as Laplace equations, such as irrotational flow of ideal fluids, electrical or magnetic potential problem, heat conduction, etc.. In this paper, therefore, we present a methodology of XFEM to solve two-dimensional Laplace equation with slit type boundaries. The basic approach is to utilize the complex velocity potential in potential flow theory.

2 FORMULATION

2.1 Governing equation

Consider the domain Ω bounded by Γ. The boundary Γ is composed of the sets Γ_1 and Γ_2 as shown in Figure 1. We solve the equation of two-dimensional Laplace equation of potential ϕ with boundary conditions as Eq.(1).

$$\begin{cases} \mu\Delta_X\phi = 0 \quad in \quad \Omega & (1a) \\ \phi = \bar{\phi} \quad on \quad \Gamma_1 & (1b) \\ \nabla_N\phi = \bar{t}_n \quad on \quad \Gamma_2 & (1c) \end{cases}$$

Where $\bar{\phi}$ is the prescribed potential of Dirichlet condition boundary, and $\bar{t}_n$ is the prescribed flux of Neumann condition boundary. Notation $\nabla_X = \{\partial/\partial X \quad \partial/\partial Y\}^T$ is a differential operator with respect to the basis vectors of the global coordinate system. Notation ∇_N is the outward directional derivative operator. Scalar μ is the permeability. As we consider the slit is flux-free, the slit boundary is included in Γ_2.

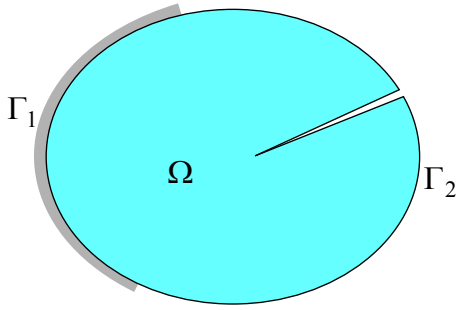

Figure 1: Domain with slit boundary

2.2 Flow around a corner of semi-infinite line

Flux, namely the gradient of potential ϕ, is compared to the flow of ideal fluid. Near the slit, flux does not penetrate the slit but proceed along the slit, and turn around the slit tip. To make XFEM framework without generating mesh conforming to the slit, we have to find a function which represents such characteristics, and use it as an enrich function. In this section, we will introduce this function. In two-dimensional Laplace equation, a complex velocity potential can be used as suitable function which represents the flux distribution around the slit.

Let consider a regular function $f(z)$. A Complex number $z = x + iy$ ($x, y \subset R$, i is imaginary unit) is mapped to a complex number $\zeta = \xi + i\eta$ ($\xi, \eta \subset R$) by $f(z)$ (Fig.2). In this case, ξ and η can be regarded as functions of both x and y. Namely,

$$\begin{cases} \xi = \Phi(x, y) & \text{(2a)} \\ \eta = \Psi(x, y) & \text{(2b)} \end{cases}$$

In the potential flow theory, this real value function Φ and Ψ are called a potential function and a stream function, respectively. They satisfy well-known Cauchy-Riemann relationship. Moreover, the equipotential line and streamline is orthogonal with each other.

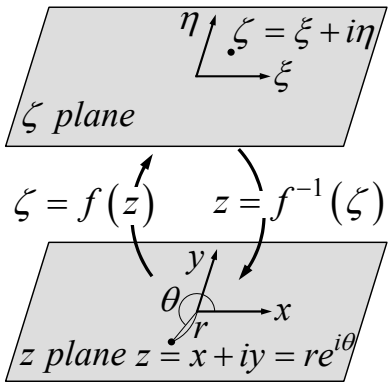

Figure 2: Mapping between z-plane and ζ-plane

Now, using positive real constant value U and n, we let $f(z)$ to be a power function of z as follows:

$$\zeta = f(z) = Uz^n \tag{3}$$

Using the representation of poler form as $z = re^{i\theta}$ and De Moivre's theorem, we obtain Eq.(4).

$$\begin{aligned} f &= Ur^n e^{in\theta} \\ &= Ur^n \cos n\theta + iUr^n \sin n\theta \end{aligned} \tag{4}$$

Then, Φ and Ψ are represented as follows:

$$\begin{cases} \Phi(x, y) = \Phi(r, \theta) = Ur^n \cos n\theta & \text{(5a)} \\ \Psi(x, y) = \Psi(r, \theta) = Ur^n \sin n\theta & \text{(5b)} \end{cases}$$

Where $r = \sqrt{x^2 + y^2}$ is radius, and θ ($0 \le \theta < 2\pi$) is argment. This type of mapping is called conformal mapping, and the angle between any two lines is kept through this mapping. Thus, the orthogonality of equipotential line and streamline is kept, and this means that the flow on the z-plane is mapped to that on the ζ-plane by this mapping. By the mapping using, $f(z)$ in Eq.(3), a steady flow on the ζ-plane is mapped to the flow around a corner of a wedge of angle π/n on the z-plane.

Now, let $U = 1$ and $n = 1/2$ for Eq.(4), then we obtain a function ϕ^e as Eq.(6)

$$\phi^e(x, y) = \phi^e(r, \theta) = \sqrt{r}\cos(\theta/2) \tag{6}$$

This function $\phi^e(\mathbf{x})$ is regarded as a potential of two-dimensional flow around a corner of semi-infinite line which extends from origin to positive direction of x-axis on the z-plane. We

can use this function in order to represent the potential around the slit boundary. Figure 3(a) shows the distribution of ϕ^e. As can be seen, ϕ^e is discontinuous on the slit $(y=0,\ 0\le x)$.

The flux velocity $\mathbf{v}=\{v_x \quad v_y\}^T$ is obtained by differentiating ϕ^e based on the chain rule of polar coordinate system as shown in Eq.(7)

$$\begin{cases} v_x = -\dfrac{\partial \phi^e}{\partial x} = \cos\theta \dfrac{\partial \phi^e}{\partial r} - \dfrac{\sin\theta}{r}\dfrac{\partial \phi^e}{\partial \theta} = -\dfrac{1}{2\sqrt{r}}\cos\dfrac{\theta}{2} & (7a) \\ v_y = -\dfrac{\partial \phi^e}{\partial y} = \sin\theta \dfrac{\partial \phi^e}{\partial r} + \dfrac{\cos\theta}{r}\dfrac{\partial \phi^e}{\partial \theta} = -\dfrac{1}{2\sqrt{r}}\sin\dfrac{\theta}{2} & (7b) \end{cases}$$

Figure 3(b) shows the distribution of ϕ^e and its gradient vector in a domain of $-1\le x,y\le 1$. The direction of flux vectors is counterclockwise. Moreover, magnitude of the velocity approaches asymptotically to infinite at the corner of the semi-infinite line.

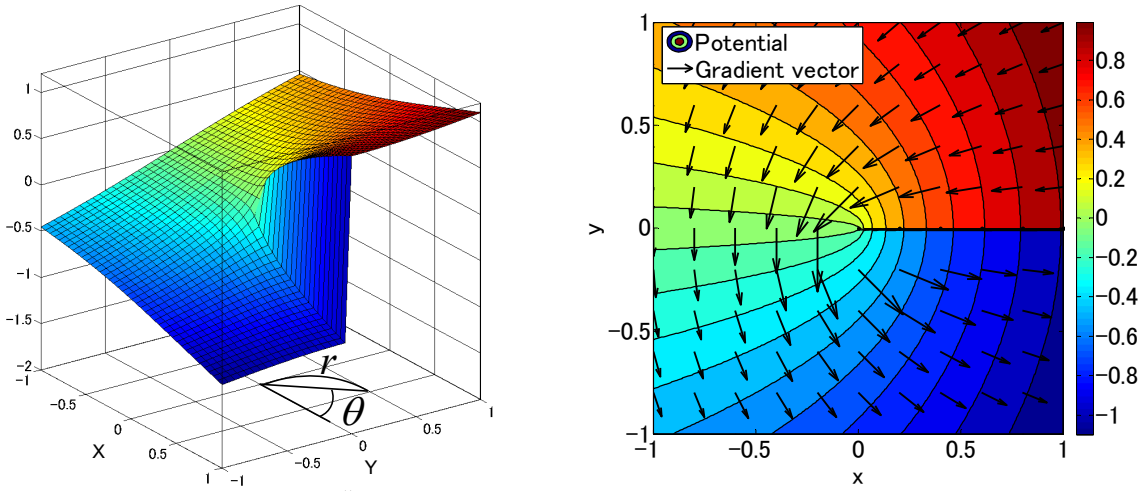

(a) Potential ϕ^e (b) Potential (contour) and flux (vector)

Figure 3: Distribution of $\phi^e=\sqrt{r}\cos(\theta/2)$

2.3 Approximation of potential based on the framework of XFEM

In this section, we introduce the approximation of potential ϕ in Eq.(1) based on the framework of XFEM. We use quadrilateral finite elements to discretize the field (Figure 4). The basic concept is to use ϕ^e noted in previous section as an enrichment function to represent the analytical distribution around a slit. Namely,

$$\phi(X,Y)=\mathbf{N}(\xi,\eta)\left\{\boldsymbol{\varphi}^n+\phi^e(x,y)\mathbf{u}\right\} \tag{8}$$

Where, $\mathbf{N}$ in Eq. (8) is a matrix, which is consisted of standard finite element shape functions $N_i\ (i=1,2,3,4)$ for the iso-parametric quadrilateral finite elements as shown in Eq. (9). The coodinate (ξ,η) is the normalized coordinate which corresponds to (X,Y), when the element domain Ω_e is mapped from physical coordinate system (X,Y) to the normalized coordinate of $-1\le\xi,\eta\le 1$.

$$\begin{aligned}\mathbf{N}(\xi,\eta) &= \begin{bmatrix} N_1(\xi,\eta) & N_2(\xi,\eta) & N_3(\xi,\eta) & N_4(\xi,\eta) \end{bmatrix} \\ &= 1/4\begin{bmatrix} (1-\xi)(1-\eta) & (1+\xi)(1-\eta) & (1+\xi)(1+\eta) & (1-\xi)(1+\eta) \end{bmatrix}\end{aligned} \tag{9}$$

And, $\boldsymbol{\varphi}^n$ and $\mathbf{u}$ are the discretized vector of ϕ^n and U, respectively. Namely, $\boldsymbol{\varphi}^n$ is the existing nodal degrees of freedom of FEM, whereas $\mathbf{u}$ is that of XFEM.

$$\boldsymbol{\varphi}^n = \begin{Bmatrix} \phi_1 & \phi_2 & \phi_3 & \phi_4 \end{Bmatrix}^T \tag{10}$$

$$\mathbf{u} = \begin{Bmatrix} u_1 & u_2 & u_3 & u_4 \end{Bmatrix}^T \tag{11}$$

In general, the slit is inclined against the global coordinate system. Since ϕ^e in Eq.(8) is defined on the coordinate system whose origin locates on the tip of the slit and the x-axis is along the slit, we have to make another coordinate system. Note that the einrich function ϕ^e should be represented on this local coordinate system.

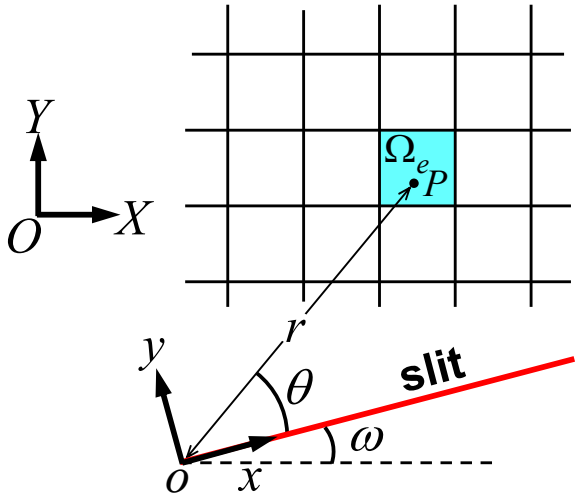

Figure 4: Configuration of slit and evaluation point

2.4 Discretized equilibrium equation

We obtain the gradient ϕ, namely $\nabla_X \phi$, by Eq. (12),

$$\begin{aligned}\nabla_X \phi &= \nabla_X \left\{ \mathbf{N}\left(\boldsymbol{\varphi}^n + \phi^e \mathbf{u} \right) \right\} \\ &= \nabla_X \mathbf{N} \cdot \boldsymbol{\varphi}^n + \left(\nabla_X \mathbf{N} \cdot \phi^e + \mathbf{N} \nabla_X \phi^e \right) \mathbf{u} \\ &= \mathbf{C} \begin{Bmatrix} \boldsymbol{\varphi}^n \\ \mathbf{u} \end{Bmatrix}\end{aligned} \tag{12}$$

Where $\mathbf{C}$ is the matrix which relates the gradient of ϕ and the nodal degree of freedom ($\boldsymbol{\varphi}^n$ and $\mathbf{u}$), and denoted by Eq. (13).

$$\mathbf{C} \equiv \begin{bmatrix} \nabla_X \mathbf{N} & \nabla_X \mathbf{N} \cdot \phi^e + \mathbf{N} \nabla_X \phi^e \end{bmatrix} \tag{13}$$

Where $\nabla_X \mathbf{N}$ in Eq.(13) is obtained as Eq.(14), and the Jacobi matrix **J** of iso-parametric mapping is obtained as Eq.(15).

$$\nabla_X \mathbf{N} = \mathbf{J}^{-1} \nabla_\xi \mathbf{N} \tag{14}$$

$$\mathbf{J} = \begin{bmatrix} \frac{\partial X}{\partial \xi} & \frac{\partial Y}{\partial \xi} \\ \frac{\partial X}{\partial \eta} & \frac{\partial Y}{\partial \eta} \end{bmatrix} = \begin{bmatrix} \frac{\partial \mathbf{N}}{\partial \xi}\mathbf{X}_e & \frac{\partial \mathbf{N}}{\partial \xi}\mathbf{Y}_e \\ \frac{\partial \mathbf{N}}{\partial \eta}\mathbf{X}_e & \frac{\partial \mathbf{N}}{\partial \eta}\mathbf{Y}_e \end{bmatrix} \tag{15}$$

Where $\nabla_\xi \mathbf{N} = \{\partial \mathbf{N}/\partial \xi \quad \partial \mathbf{N}/\partial \eta\}^T$ in Eqs.(14) and (15) is obtained explicitly from Eq.(9), and the nodal coordinate vectors $\mathbf{X}_e$ and $\mathbf{Y}_e$ are represented as Eq. (16)

$$\mathbf{X}_e = \{X_1, X_2, X_3, X_4\}^T \tag{16a}$$

$$\mathbf{Y}_e = \{Y_1, Y_2, Y_3, Y_4\}^T \tag{16b}$$

The following relationship holds between (X,Y) and (ξ,η).

$$\begin{cases} X = \mathbf{N}(\xi,\eta)\mathbf{X}_e & \text{(17a)} \\ Y = \mathbf{N}(\xi,\eta)\mathbf{Y}_e & \text{(17b)} \end{cases}$$

Since ϕ^e is defined on the local coordinate system, we obtain $\nabla_X \phi^e$ in Eq.(13) by Eq.(18).

$$\nabla_X \phi^e = \mathbf{L} \nabla_x \phi^e \tag{18}$$

Where **L** in Eq.(18) is a coordinate transform matrix which transforms arbitrary vectors from the local coordinate system *oxy* into the total coordinate system *OXY* , and **L** is discribed as Eq. (19).

$$\mathbf{L} = \begin{bmatrix} \cos\omega & -\sin\omega \\ \sin\omega & \cos\omega \end{bmatrix} \tag{19}$$

Moreover, $\nabla_x \phi^e = \{\partial \phi^e / \partial x \quad \partial \phi^e / \partial y\}^T$ is denoted in Eq.(7).

After some manupulation, using the weighted residual method, we obtain the discretized equiriburium equations as follows:

$$\mathbf{K}\boldsymbol{\varphi} = \mathbf{f} \tag{20}$$

$$\mathbf{K} = \sum \mathbf{K}_e, \quad \boldsymbol{\varphi} = \sum \begin{Bmatrix} \boldsymbol{\varphi}^n \\ \mathbf{u} \end{Bmatrix}, \ \mathbf{f} = \sum \begin{Bmatrix} \mathbf{f}_e \\ \mathbf{0} \end{Bmatrix} \tag{21a,b,c}$$

Where, $\sum$ means the sum of elements and/or element boundaries. The element stiffness matrix $\mathbf{K}_e$ is specifically calculated in Eq.(22)

$$\begin{aligned} \mathbf{K}_e &= \int_{\Omega_e} \mu \mathbf{C}^T \mathbf{C} d\Omega_e \\ &= \iint \mu \mathbf{C}^T \mathbf{C} dX dY \end{aligned} \tag{22}$$

As the integrant in Eq.(22) is discontiuous on the slit line, it is desirable to sub-devide elements on the slit into some triangles, and integrate them separately, as well as the way for XFEM enriched with Heaviside function. However, this process needs complicated geometric handling. Thus, in our reserch, we used higher order approximation for standard gauss integral scheme as shown in Eq.(23). We used parameter $n = 4$ for the elements which include enriched nodes.

$$\begin{aligned}\mathbf{K}_e &= \int_{-1}^{1}\int_{-1}^{1} \mu \mathbf{C}^T \mathbf{C} |\mathbf{J}| d\xi d\eta \\ &= \sum_{i=1}^{n}\sum_{j=1}^{n} \mu \mathbf{C}\left(\xi_i, \eta_j\right)^T \mathbf{C}\left(\xi_i, \eta_j\right) |\mathbf{J}| w_i w_j\end{aligned} \tag{23}$$

3 NUMERICAL EXAMPLE

In this chapter, we demonstrate a simple example. Figure 5 shows the analysis model. The square domain is discretized into 18×18 orthogonal grid type finite elements. Potential is prescribed on the boundary parallel to the X-axis. On the boundary parallel to the Y-axis, flux is prescribed to zero as Neumann boundary condition. Slit boundary is included in this Neumann boundary condition, and it is not represented on the mesh. The inclination angle of the slit is 30 degree to the X-axis.

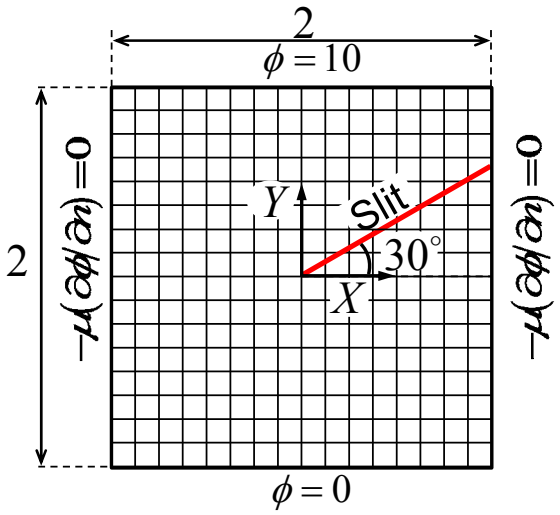

Figure 5: Analysis model

Figure 6 shows the configuration of the enriched nodes. Elements with yellow color have more than one enriched node, and these elements are numerically integrated using 4×4 points for calculation of element stiffness matrix $\mathbf{K}_e$ in Eq.(23). In the case of XFEM using Heaviside step function as enrichment function, only elements including the slit (discontinuous segment) have the enriched node. Excessive nodal enrichment leads to ill-conditioned stiffness matrix. In our case study using the enrich function in Eq.(6), however, suitable solutions were obtained even if the enriched nodes were distributed over the larger

domain. This leads to the flexibility of algorithm searching enriched nodes.

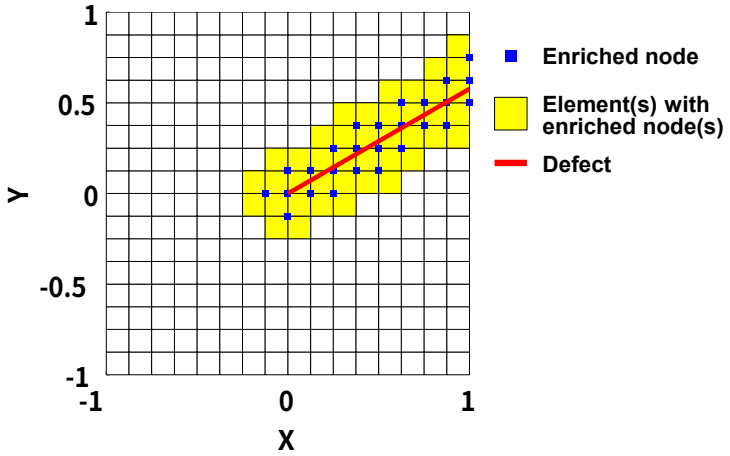

Figure 6: Configuration of enriched node and element with enriched nodes

We will verify the obtained solution. Figure 7 shows the distribution of potential ϕ. This value plotted on each integral point calculated in Eq.(17). Next, the solution ϕ is decomposed. Figure 8 shows the distribution of $\mathbf{N}\boldsymbol{\varphi}^n$. This value corresponds to the classical finite element component of ϕ. We can see that this value is distributed continuously. On the other hand, the potential derived from enrichment, namely $\mathbf{N}\phi^e\mathbf{u}$ shown in Figure 9, represents the discontinuity around the slit.

Figure 10 shows the distribution of enriched nodal degree $\mathbf{Nu}$. The magnitude of this value becomes large as it approaches the slit boundary. Since the flux is counterclockwise around the slit, this value is positive. In the case of clockwise, this value takes negative value.

Figure 11 shows the distribution of flux vector (gradient of potential). As the original value is obtained on each integral point, they are interpolated so as to evaluate on the center of each element.

4 CONCLUSIONS

- A technique of XFEM framework for two-dimensional Laplace equation with slit boundaries is proposed. Real part of the power function of complex number which shows the flow around a corner of a semi-infinite plate in potential flow theory is used as enrichment function.

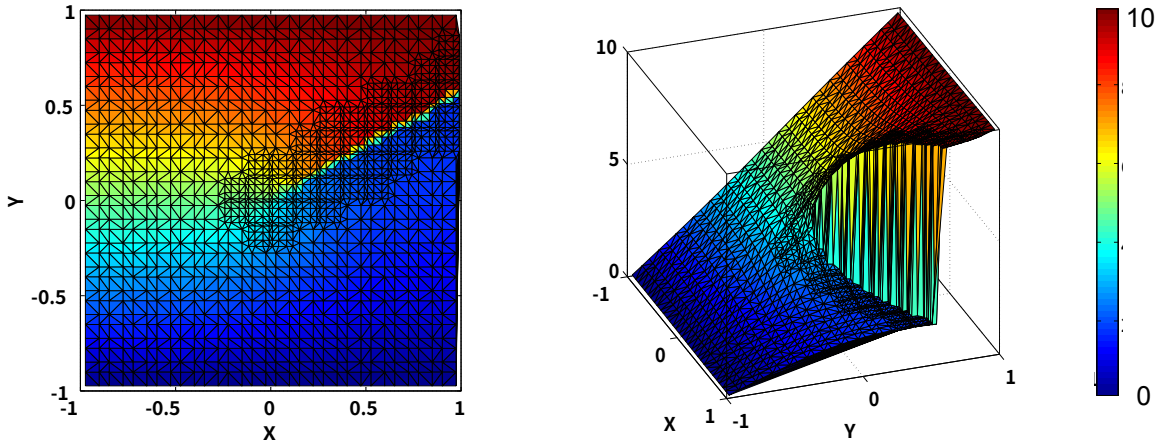

(a) Overview (b) Bird's eye view

Figure 7: Distributino of potential (Total component)

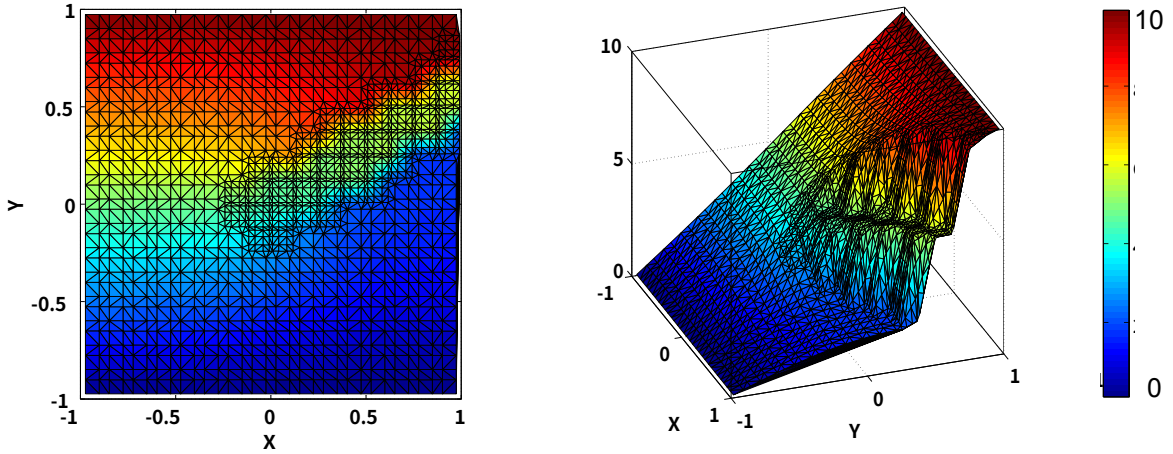

(a) Overview (b) Bird's eye view

Figure 8: Distributino of potential (Nomal component)

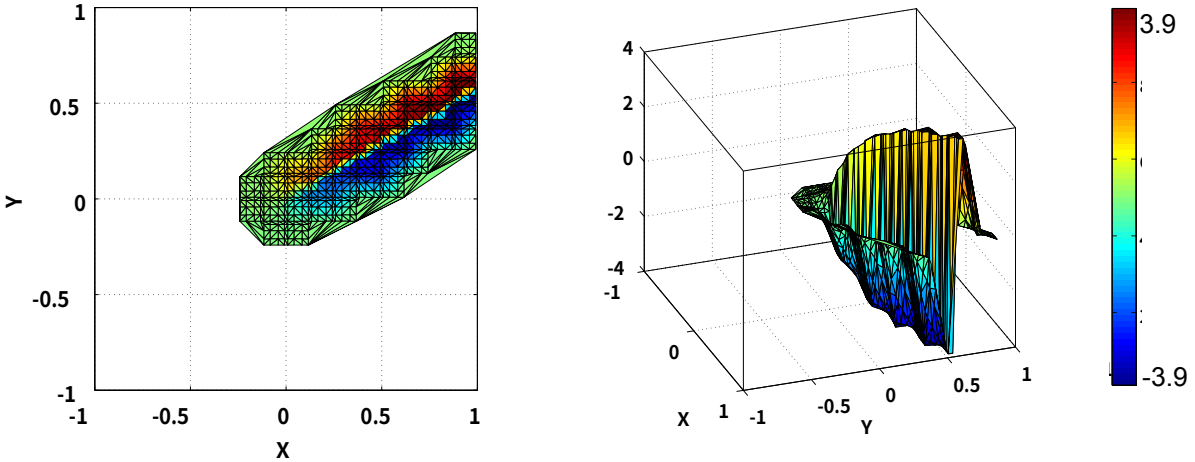

(a) Overview (b) Bird's eye view

Figure 9: Distributino of potential (Enriched component)

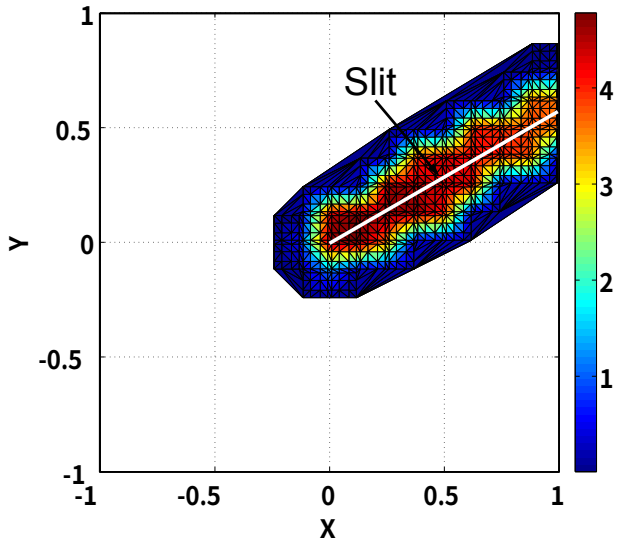

Figure 10: Magnitude of enriched nodal degree

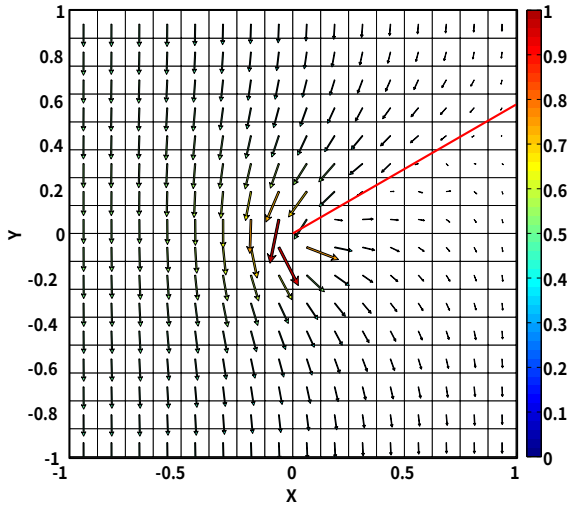

Figure 11: Flux vector

REFERENCES

[1] Belytschko T. Moes, N. Usui S. and Parimi C. Arbitrary discontinuities in finite elements, *Int.J. Numer. Meth. Engng* (2001) **50**:993-1013.

[2] Moes, N. Dolbow, J. and Belytschko, T. A finite element method for crack growth without remeshing, *Int. J. Numer. Meth. Engng* (1999) **46**:131-150.

[3] Dolbow, J Moes, N. and Belytschko T. Discontinuous enrichment in finite elements with a partition of unity method, *Finite Elements in Analysis and Design* (2000) **36**:235-260.

[4] Belytschko T. Black T. Elastic crack growth in finite elements with minimal remeshing, *Int.J. Numer. Meth. Engng* (1999) **45**(5):601-620.

[5] Mohammadi, S. *Extended Finite Element Method*, Blackwell Publishing (2007).
[6] Yazid, A. Abdelkader, N. and Abdelmadjid, H. A state-of-the-art review of the X-FEM for computational fracture mechanics, *Applied Mathematical Modelling* (2009)**33**:4269-4282.
[7] Melenk, J. and Babuska, I. The partition of unity finite element method: Basic theory and applications. *Comput. Methods Appl. Mech. Engng* (1996) **139**:289-314.
[8] Sukumar, N. Chopp, D.L. and Moran B. Extended finite element method and fast marching method for three-dimensional fatigue crack propagation, *Engineering Fracture Mechanics* (2003) **70**:29-48.
[9] Sukumar, N. Chopp, D.L. Moes, N and Belytschko T. Modeling holes and inclusions by level sets in the extended finite-element method, *Comput, Methods Appl. Mech. Engrg*. (2001)**190**:6183-6200.
[10] Nagashima T. Omoto Y. and Tani S. Stress intensity factor analysis of interface cracks using X-FEM, *Int. J. Numer. Meth. Engng* (2003) **56**:1151–1173.
[11] Elguedj, T. Gravouil, A. and Combescure, A. Appropriate extended functions for X-FEM simulation of plastic fracture mechanics, *Comput. Methods Appl. Mech. Engrg.* (2006)**195**:501-515
[12] Sawada, T. and Tezuka, A. LLM and X-FEM based interface modeling of fluid‐thin structure interactions on a non-interface-fitted mesh, *Comput Mech* (2011) **48:**319-332.
[13] Gerstenberger, A. and Wall, W. A. An eXtended Finite Element Method/Lagrange multiplier based approach for fluid–structure interaction, *Comput. Methods Appl. Mech. Engng*. (2008) **197:** 1699–1714.